Stress Induced Matrix Microcracking in Brittle Matrix Plain Weave Fabric Composites Under Uniaxial Tension

J. L. KUHN, S. I. HAAN AND P. G. CHARALAMBIDES[1]
Department of Mechanical Engineering
The University of Maryland, Baltimore County
1000 Hilltop Circle
Baltimore, MD 21250

(Received January 21, 1999)
(Revised September 6, 1999)

ABSTRACT: A stress induced microcracking non-linear model is employed as part of an incremental and iterative hierarchical modeling procedure aiming at studying the evolution of damage in brittle matrix plain weave fabric composites, subjected to uniaxial tension. The study focuses exclusively on matrix micro-damage and its effects on the macroscopic non-linear woven composite response. For a given load increment, the requisite microstresses and associated state of matrix microcracking are updated through an iterative converging procedure that employs the woven microstress analysis model of Kuhn and Charalambides and the discrete microcracking model employed by Charalambides and McMeeking. While matrix microcracking is predicted in regions of high stress concentration at the early stages of loading, its non-linear effects on the macroscopic stress-strain curve were shown to become visible at applied normalized strain $\hat{\varepsilon}_x \approx 1$. At about the same level of applied loading, the composite effective elastic in-plane properties in the loading and transverse directions were shown to degrade non-uniformly, thus resulting in damage induced macroscopic elastic anisotropies. The evolution of matrix micro-damage with the applied load was shown to initially take place within well defined, relatively narrow bands in regions of high stress concentration. With applied load increases, the matrix microcracking zones were shown to spread outward from the center of the unit-cell within a confined region thus forming macroscopic damage zones consistent with discrete micro-fracture events such as inter-bundle matrix cracking, bundle mode I cracking, and bundle transverse matrix cracking. The results are compared with experimental results presented by Aubard, Lamon, and Allix for a brittle matrix system with similar matrix and fiber material, but less complex microstructure.

[1]Author to whom correspondence should be addressed.

0021-9983/00/19 1640–25 $10.00/0 DOI: 10.1106/6RD6-PHGE-6RWU-NBW8

INTRODUCTION

WOVEN FABRIC REINFORCED Ceramic Matrix Composites (CMCs) may exhibit significantly higher fracture toughness than monolithic ceramics, while retaining the desirable mechanical properties such as stiffness, strength, oxidation and creep resistance. This may be the main reason why woven CMCs are being currently used in components exposed to rather extreme loading environments such as the combustion chamber and throat regions of advanced upper stage, booster/core rocket systems, and most recently in nuclear fusion reactions. The resistance to brittle failure observed in woven CMCs is a consequence of the highly complex microstructure which may help activate multipe stress-induced damage mechanisms, resulting in a non-linear macroscopic constitutive response as observed by several researchers [1–10]. The apparent "ductility" of woven CMCs is associated with energy dissipation during a cycle of loading. Numerous experimental studies on the macroscopic response of brittle matrix woven systems have been presented in the literature [1–13].

According to the experimental studies of Bordia et al. [12], and Nair and Wang [11], continuous fiber reinforced woven composites comprised of brittle fibers and a ceramic matrix have been shown to exhibit enhanced resistance to macroscopic crack growth. A process zone consisting of microcrack formation and fiber bridging was observed ahead of the crack tip in each of the above studies. A detailed study of the evolution of damage of similar systems was presented by Wang et al. [3], where experimental evidence of localized matrix microcracking, fiber fracture, delamination between layers, and fiber pull-out was reported. Other types of localized damage including bundle transverse cracking and fiber and bundle coating fracture have been observed by Steyer and Zok [13] and McNulty and Zok [10]. The experimental study presented by Aubard et al. [6] illustrates the presence of inter-tow matrix microcracking as well as microcracking of the matrix phase within the woven fiber bundles.

While the experimental characterization of woven CMCs is now well under way, there has been a relatively limited amount of work in modeling the non-linear response of such systems [2,4,6,8,14,15]. In addition, most reported models do not fully incorporate the complex woven composite microstructure while also relying on rather simplistic assumptions regarding the actual micro-strain distribution under remote loading. A reliable prediction of both the linear and non-linear response of fabric reinforced composites depends critically on the ability to accurately describe the woven unit-cell geometry, which is needed in the derivation of accurate micro-strain distributions. A few researchers [16–18] have developed 3-D finite element models to compute the distributions of micro-strains in woven systems. Most of these studies, however, involve computationally intensive calculations which limit their use to mostly the elastic regime. In recent studies, Kuhn and Charalambides [19,20] developed a semi-analytical approximate model capable of predicting the elastic micro-strain and micro-stress fields in woven composites under a general in-plane loading condition. This computationally efficient model compared favorably to 3-D finite element models [21]. The damage model employed herein relies heavily on the use of the Kuhn and Charalambides micro-stress predictive model. As will be discussed in greater detail later on in this work, the micro-stress semi-analytic model is employed during every iteration within each load increment as needed to update the micro-strain fields and the requisite state of micro-damage.

The non-linear macroscopic response model presented herein is built on the foundation of five hierarchical sub-models. At the micro-structural level as presented in Figure 1, micromechanics models employed in References [22,23] are used to predict the response of the effective tows and inter-tow matrices. At the meso-mechanical level, unit-cell geometry models presented in Reference [24] are employed as needed for the accurate 3-D topological description of the rather complex woven unit-cell architecture. At the macro-mechanical level, the models presented in References [19,22,23] capable of predicting the effective linear elastic response and woven unit-cell elastic micro-fields are also employed. A key aspect to predicting the onset and growth of damage is the distribution of the micro-strains under remotely applied loading. As discussed earlier, the micro-strains are computed using a semi-analytical method or approximation presented in Reference [19]. The computational efficiency of the above method is demonstrated via several case studies presented in References [20,21,25].

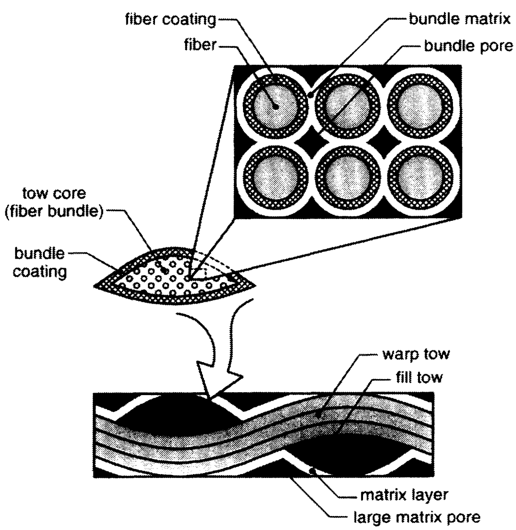

Figure 1. *Schematic of a typical Chemical Vapor Infiltrated (CVI) ceramic matrix plain weave fabric composite microstructure.*

The stress-induced microcracking continuum model used in this study to monitor the evolving state of damage was first developed by Charalambides and McMeeking in References [26,27]. The model consists of degrading the material properties with increasing microcrack density based on the results of Budiansky and O'Connell [28]. The microcracking law which governs the microcrack density as a function of an effective stress measure is used in conjunction with the orthotropic stress-strain relation to yield a locally isotropic constitutive response similar to that presented by Fu and Evans [29].

The CVI woven ceramic matrix composite under consideration is comprised of a Nicalon fiber and SiC matrix. We assume that the matrix material located outside the bundle volume as well as that internal to the bundles microcracks at a scale that can be modeled as a continuum. Thus, in this study the above models aimed at predicting the linear response at each incremental step of loading, shall be used in conjunction with the microcracking continuum model in an iterative scheme to simulate the non-linear macroscopic stress-strain behavior of a plain weave unit-cell under remotely applied uniaxial tension.

GENERAL MODELING APPROACH

The woven microstructure gives rise to a highly complex micro-stress field which may induce numerous micro-fracture events including interbundle matrix cracking, transverse bundle matrix cracking and bundle mode-I matrix cracking. Other types of damage such as bundle delamination, microcracking of other constituent phases, crack bridging and fiber pull-out may also occur with increasing loading. In this work, the emphasis is placed on the first three of the above micro-fracture events which are known to play a key role in the early stages of failure of woven CMCs under remote tension loading.

The non-linear macroscopic stress-strain curve of the matrix microcracking woven unit-cell under uniaxial tension is simulated by employing an analytical linear model within an incremental and iterative scheme. At a given state of remote loading, the linear model, which utilizes the current values of the degraded elastic effective properties of the matrix, can be used to compute the local micro-stresses. These stresses are then used to update the state of damage, which results in further degradation of the effective properties of the matrix. This process is repeated until one of the field quantities such as the stress or state of damage converges to within a specified limit.

Elastic Micro-Fields in the Woven Unit-Cell

The woven unit-cell geometry model used for this analysis is the matrix layer model presented in Reference [24]. In this model, the woven composite is treated as a composite laminate with four non-uniform layers. Extensive discussion on each of the geometry features as well as a detailed presentation of the functions used to represent the top and bottom surface of each layer can be found in Reference [24].

The woven unit-cell is comprised of the warp tows, fill tows, and inter-tow matrix phases at the mesoscopic scale as shown in Figure 1(a). A rigorous hierarchical micromechanics model utilizing the Hashin [30] Composite Cylinder Assemblage (CCA) model and porous solid model employed by Bassani [31], aimed at homogenizing each phase and predicting the effective elastic tow response in terms of the bundle constituent properties was used for this study and was presented comprehensively in Reference [22].

The boundary value problem under consideration is that associated with uniaxial tension in the x-direction. The remotely applied uniaxial loading F_x^∞ on a woven ply is simulated with the approximate symmetry and displacement boundary conditions applied to the symmetric woven unit-cell. The above boundary condition is discussed in detail in Reference [19].

The unit-cell geometry, material properties, and boundary conditions outlined above constitute an elasticity boundary value problem in three dimensions. The problem is reduced to a two-dimensional plate elasticity boundary value problem by employing the Kirchhoff-Love deformation hypothesis and approximate analytical solutions are obtained by the Rayleigh-Ritz method which is presented in great detail in Reference [19].

Stress Induced Matrix Microcracking Model

As discussed elsewhere [3,6] and summarized earlier in this study, CVI ceramic matrix woven composites are known to sustain multiple types and rather extensive damage prior to catastrophic failure. In accordance with the stress-strain curve shown in Figure 2, matrix related cracking may indeed play an important role throughout the loading history and may critically control the onset of non-linearities in the stress-strain response of CVI ceramic matrix composites. As in unidirectionally fiber reinforced CMCs, during loading, the fiber bundles or tows may experience either transverse matrix cracking or even matrix cracking in a direction orthogonal to the fiber reinforcements. Such cracking phenomena have been studied rather rigorously using shear lag type models or even other meso-mechanical models, that often rely on the fiber and matrix properties, fiber volume fraction, and fiber/matrix inter-facial shear strength properties. The above models are often used to predict the macroscopic cracking stress as well as to predict the macroscopic non-linear stress-strain response of the fiber reinforced composite as a function of cracking density or spacing [32]. While the models were shown to provide great insights on the failure behavior of unidirectional CMC systems under a uniaxial state of stress, their relative complexity does not allow for their effective use in an environment of multi-axial stress states, such as that dominating

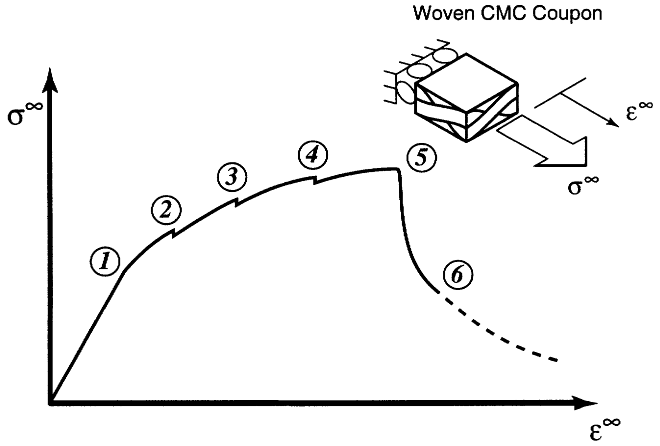

Figure 2. *Schematic representation of a non-linear stress-strain curve for a CVI brittle matrix woven composite. The critical points on the above curve represent the onset of potential damage such as (1) interbundle matrix cracking, (2) bundle transverse matrix cracking, (3) bundle mode-I cracking, (4) bundle delamination, (5) fiber pull-out and formation of a major crack, and (6) crack surface separation and loss of load bearing capacity.*

the fiber reinforced woven tows in CMC woven systems. The complexity in evaluating cracking in the latter systems further increases by the fact that non-linear interactions resulting from the various types of potential micro-constituent damage may also play a key role in the damage evolution and non-linear behavior of woven CMCs.

In light of the above almost daunting task of evaluating stress induced damage in woven CMCs with complex microstructures, we employ herein a rather simple continuum modeling approach, which, as will be shown later on, nicely captures most of the effects related to micro-failures in the matrix phase of the woven composite. More specifically, in this work, a continuum stress-induced microcracking damage model is employed as needed to evaluate the state of matrix damage at all relevant points in the interior of the woven unit-cell. Thus, the continuum model requires as an input, the current state of micro-stress or micro-strain dominating the matrix material in the unit-cell. As discussed above, such micro-field estimates are now readily obtainable via the Kuhn and Charalambides semi-analytical model that employs the Rayleigh-Ritz method of approximation. As a result, the Kuhn and Charalambides micro-field model is now being combined with the stress-induced microcracking model employed by Charalambides and McMeeking to evaluate the state of matrix damage in woven CMCs. The two models are being used as part of an incremental loading scheme aiming at establishing the non-linear stress-strain responses of CMCs attributed to matrix related damage. For the sake of completeness, the Charalambides and McMeeking model shall be presented next.

THE MICROCRACKING CONTINUUM

The microcracking continuum model employed herein is that developed by Charalambides and McMeeking [26,27]. The model is founded on the work of Fu and Evans [29] who studied the evolution of discrete microcracking at grain facets in polycrystalline ceramics. Their findings suggested that an effective stress measure such as that used in Reference [26], can be used to update the microcrack density ε, as defined by Budiansky and O'Connell [28], at every point in the solution domain. The microcracking law shown schematically in Figure 3 was first suggested by Fu and Evans [29] and was later employed by Charalambides and McMeeking [26,27], in their near-tip stress-induced microcracking and toughening studies of brittle microcracking solids. The use of the above model in studies aiming at addressing toughening in a specific system such as the polycrystalline alumina system, was initially and may still be viewed with skepticism. Even today, it is arguable as to whether indeed such a system is toughened through the development of a discrete microcracking zone in the crack-tip region or whether other mechanisms such as crack deflection and large grain bridging are the main toughening agents in the above systems. Recognizing the diversity of scientific opinions on the use of such a continuum model as a means of predicting the non-linear mechanical response of specific material systems, the authors would like to emphasize that the microcracking model employed herein is used only as a simple but effective tool to account for the material stiffness degradation at a point as a function of the associated stress state.

The implementation of the microcracking model and parametric studies presented in this work are performed through the independent model parameters such as the microcracking rate constant λ, the first microcracking critical stress σ_c, the saturation microcracking stress σ_m and saturation microcracking density ε_s. The association of the above parameters to specific material systems would need to be

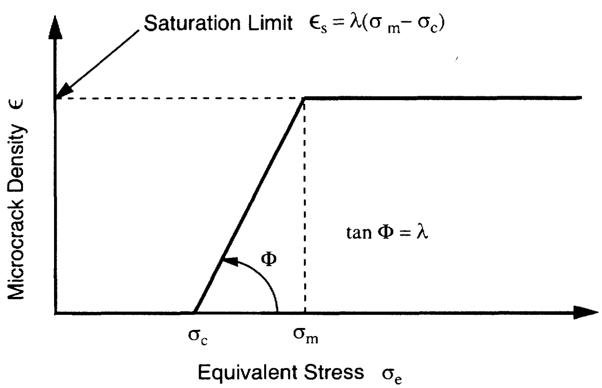

***Figure 3.** Microcracking law relating microcrack density with equivalent stress.*

established with the aid of model experiments that include mechanical testing of woven tensile coupons as well as micro-structural characterization needed to associate the extent and degree of damage to the requisite non-linear stress-strain curve. Although critical in our effort to understand, quantify and predict the mechanical response of such complex systems with intricate microstructures, the latter objective extends well beyond the scope of this study and is thus not addressed herein. In light of the above, we shall now proceed to present the adopted stress-induced microcracking model.

As discussed above, the microcracking model is comprised of a microcracking law which relates the current state of stress to the current state of microcracking damage. As shown in Figure 3, the discrete microcrack density ε is obtained as a function of stress as follows:

$$\varepsilon = \begin{cases} 0 & \text{for } \sigma_e < \sigma_c \\ \lambda(\sigma_e - \sigma_c) & \text{for } \sigma_c \le \sigma_e \le \sigma_m \\ \varepsilon_s = \lambda(\sigma_m - \sigma_c) & \text{for } \sigma_m < \sigma_e \end{cases} \tag{1}$$

where ε is the microcrack density as defined by Budiansky and O'Connell [28], and $\sigma_e = \sqrt{\sigma_{ij}\sigma_{ij}}$ is an equivalent stress. The parameters σ_c and σ_m represent the equivalent stresses at which microcracking initiates and subsequently becomes saturated, respectively. The saturation microcrack density is denoted by ε_s and λ is the microcracking rate. Charalambides and McMeeking [27] approximated the Budiansky and O'Connell [28] expressions for the effective elastic properties of a microcracking solid as follows:

$$\frac{\bar{E}}{E} = \frac{\bar{\nu}}{\nu} = 1 - \frac{16}{9}\varepsilon = \frac{1}{f} \tag{2}$$

where $\bar{E}$ and $\bar{\nu}$ are the effective Young's modulus and Poisson's ratio of the microcracked solid, respectively, and E and ν represent the properties of the uncracked solid. The microcracking parameter f is defined as an internal state variable for convenience. Consistent with the above, the stress-strain relationships for the microcracking solid for planar problems takes the form [19]:

$$\sigma_{\alpha\beta} = \frac{E}{f + \nu^*}\left[\varepsilon_{\alpha\beta} + \frac{\nu^*}{f - \nu^*}\varepsilon_{\gamma\gamma}\delta_{\alpha\beta}\right] \alpha, \beta, \gamma = 1, 2 \tag{3}$$

where $\nu^* = \nu$ for plane stress and $\nu^* = \nu/(1 - \nu)$ for plane strain. In the above expression, repeated indices in a product imply summation over that index from 1 to 2. Also in Equation (3), $\delta_{\alpha\beta}$ is the Kronecker delta in two dimensions which takes the value of 1 when $\alpha = \beta$ or 0 when $\alpha \neq \beta$.

A schematic drawing of a uniaxial stress-strain curve that obeys Equation (3) is shown in Figure 4. As shown, the material loads linearly without loss of stiffness at

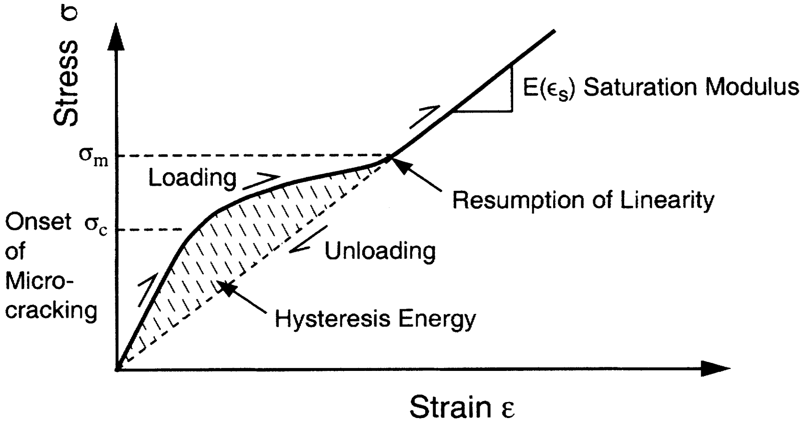

Figure 4. *The profile of the non-linear stress-strain curve associated with the sub-critical and isotropic microcracking continuum.*

all points wherein the effective stress σ_e is less than or equal to σ_c. Once exceeded, the microcrack density ε increases linearly with σ_e, consistent with the microcracking law given in Equation (1) and shown in Figure 3. Thus, upon the initiation of microcracking, ε becomes non-zero which leads to material stiffness degradation consistent with Equation (2). The non-linear branch of the stress-strain curve, shown in Figure 4, is clearly associated with the continual material loss of stiffness, until the effective stress at the point of interest σ_e reaches or exceeds the saturation stress σ_m of the microcracking continuum. As will be shown later on in this work, the above microcracking conditions lead to smooth transitional damage zones between the undamaged and fully damaged material. This condition is referred to as sub-critical microcracking. Upon loading, the system unloads linearly along a path dictated by the degraded stiffnesses to zero stress for zero strain. Clearly the adopted stress-strain law does not account for residual strains that may potentially result due to residual microcrack opening caused by either thermal processing stresses or even by microstructure events such as fiber failure and frictional fiber pull-out.

For a given state of strain at a point in the microcracking material under monotonically increasing loading, the above set of non-linear equations can be used to compute the corresponding local damage f. The second line in Equation (1) represents the non-linear segment of the response. Hence, we seek a solution f to the equation

$$F(f) = \lambda(\sigma_e - \sigma_c) - \frac{9}{16}\left(1 - \frac{1}{f}\right) = 0 \qquad (4)$$

in the interval

$$1 \le f \le \left(1 - \frac{16}{9}\varepsilon_s\right)^{-1} \tag{5}$$

If the computed value of *f* falls outside the above interval, the appropriate bound is chosen as the solution. The equivalent stress can be written in terms of the local strains under phase stress conditions as

$$\sigma_e = \frac{E}{f^2 - \nu^2}\alpha^{1/2} \tag{6}$$

where the variable α is defined in terms of *f* and the strains as follows

$$\alpha(f) = (f^2 + \nu^2)(\varepsilon_x^2 + \varepsilon_y^2) + 4\,\nu\, f\, \varepsilon_x\, \varepsilon_y + \frac{1}{2}(f - \nu)^2\, \gamma_{xy}^2 \tag{7}$$

and for convenience the derivative of $\alpha(f)$ with respect to *f* denoted as β is given by

$$\beta(f) = \alpha'(f) = 2f(\varepsilon_x^2 + \varepsilon_y^2) + 4\,\nu\,\varepsilon_x\,\varepsilon_y + (f - \nu)\,\gamma_{xy}^2 \tag{8}$$

The characteristic equation used to compute the damage parameter *f* may then be rewritten as

$$F(f) = E\,\alpha^{1/2} + (f^2 - \nu^2)\left[\frac{9}{16\lambda}\left(\frac{1}{f} - 1\right) - \sigma_c\right] = 0 \tag{9}$$

and the respective derivative is given by

$$F'(f) = \frac{E}{2}\alpha^{-1/2}\,\beta + \frac{9}{16\lambda}\left(\frac{\nu^2}{f^2} - 2f + 1\right) - 2\,f\,\sigma_c \tag{10}$$

For a given state of strain, the functions $F(f)$ and $F'(f)$ may then be used in the Newton-Raphson method to compute the microcracking state variable *f*.

As the material is subjected to an arbitrary loading sequence, the microcrack density ε and damage parameter *f* may not decrease even as the material is unloaded. In the present case the properties E and ν represent the inter-bundle and bundle matrix properties E_m and ν_m respectively. Consequently, the degraded effective microcracked matrix properties are thus denoted as $\bar{E}_m$ and $\bar{\nu}_m$.

As was mentioned earlier, the microcracking model can be used to compute the distribution of damage within the unit-cell given the micro-strain field computed by the Rayleigh-Ritz method. This results in degraded material properties of the inter-tow and bundle matrix materials. This completes the hierarchical model which is used to compute the micro-structural damage in the matrix material for a specified loading. In the next section the sequence outlined above will be embedded in an iterative scheme to trace the macroscopic non-linear stress-strain curve of the brittle matrix woven composite.

Non-Linear Response

In order to obtain the relationship between the applied stress σ^∞ to the resulting macroscopic strain ε^∞, a strain controlled secant incremental and iterative scheme is employed as shown in Figure 5. Initially the woven unit-cell is assumed to be unloaded with no residual stresses. In accordance with this scheme the unit-cell is loaded incrementally by applying a remote strain. The schematic diagram shown in Figure 5 illustrates the procedure used to trace the uniaxial non-linear response of the woven unit-cell. As shown, at load increment i, a remote strain of ε^i is applied to the unit-cell. At iteration j the Rayleigh-Ritz method is used to compute the effective unit-cell modulus $\bar{E}^i_j$, the remote stress σ^i_j, and the local distribution of strain in the unit-cell. Using this local strain-field and the constitutive law presented earlier, the local damage f^i_j in the matrix material of each layer is computed at discrete integration points throughout the unit-cell. The damage magnitudes are not allowed to drop below the final damage f^{i-1} of the prior load increment.

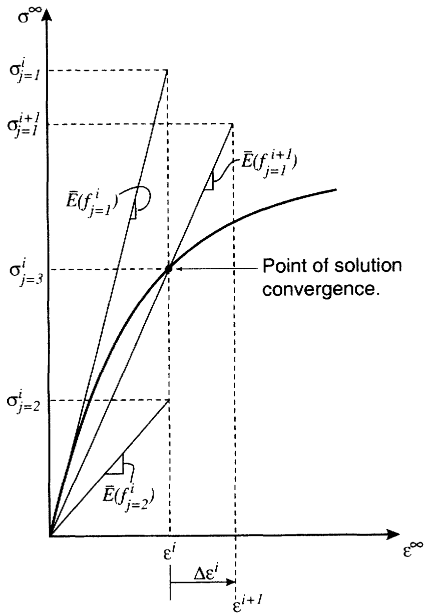

Figure 5. *The secant approach to tracing the non-linear stress strain curve. In this schematic, convergence is shown to be achieved over* j = *3 iterations.*

In the next iteration, $j + 1$, the local damage f_j^i is used to further degrade the matrix material properties. The new degraded properties are then employed by the linear model to compute the requisite effective response of the damaged unit-cell, which is now associated with a remote stress σ_{j+1}^i. The process is repeated until the damage parameter converges. The final stress σ^i from load step i is stored, the strain is incremented by $\Delta\varepsilon^i$, and the iterative process outlined above is repeated. The applied strain is incremented several times until the full strain is applied.

In the model implementation, a Gauss integration scheme is employed to compute the stiffness terms of the Rayleigh-Ritz method. Eight isoparametric domain elements as shown in Figure 6(a) are introduced as needed to accurately compute the high stress gradients in the vicinity of the pre-existing void as discussed elsewhere [19]. Within each domain element, a user-controlled $M \times N$ number of integration stations are allowed consistent with Rayleigh-Ritz method convergence studies reported in Reference [19]. Multiple, also user-controlled n_z number of integration stations are introduced for stiffness and damage updates in the thickness z-direction as shown in Figure 6(b). As a result, a total of $8 \times M \times N \times n_z$ number of integration stations are used to evaluate the Rayleigh-Ritz method volume integrals. At the end of each load increment, the local-degraded stiffness and associated damage parameter are stored at each of the integration stations (Figure 7).

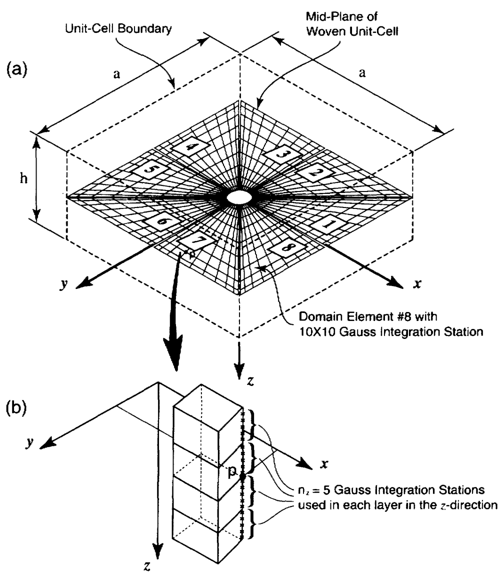

Figure 6. *(a) The x-y grid of Gauss integration stations used in the calculation of the volume integrals of the Rayleigh-Ritz method developed in Reference [19]. (b) Integration in the out-of-plane z-direction is carried out using a user-controlled* n_z *number of Gauss points within each layer as shown above.*

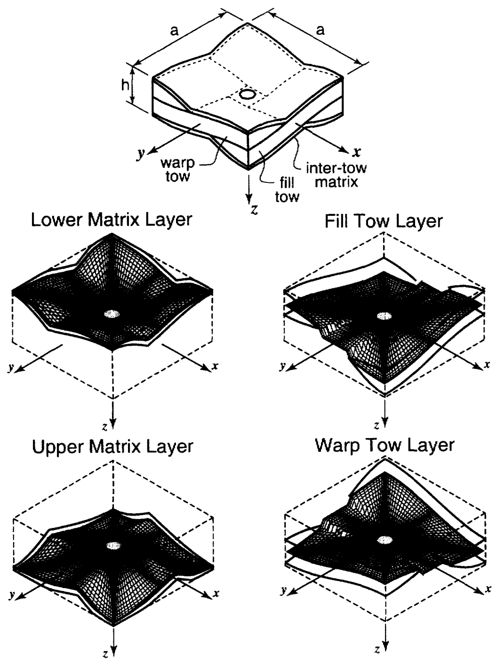

Figure 7. *Gaussian integration station locations within each layer used to compute the volume integrals associated with the Rayleigh-Ritz method developed in Reference [19]. For clarity purposes, only one integration station layer is shown above within each layer.*

MICROCRACKING SIMULATIONS

A computer program module was developed to perform the non-linear analysis procedure outlined in the previous section. The module was incorporated into the DENDRO graphical user-friendly technology transfer software package developed by Charalambides and Kuhn.

The computations were completed in a non-dimensional environment. In this context, spatial dimensions including length and position are normalized by a characteristic length $L_c = a$, such that the non-dimensional unit-cell half period $\hat{a} = a / L_c = 1.0$. The shear and Young's moduli of each micro-constituent, mesoscopic phase, and the overall unit-cell are normalized by a characteristic modulus $E_c = E_m$, which yields a non-dimensional matrix modulus of $\hat{E}_m = E_m / E_c = 1.0$. Stress components are normalized by a characteristic stress Σ_c equal to the matrix microcracking initiation stress σ_c. As a result the non-dimensional bulk matrix material critical microcracking stress is given by $\hat{\sigma}_c = \sigma_c / \Sigma_c = 1.0$. The characteristic strain Υ_c is related to the characteristic stress Σ_c and the characteristic modulus E_c through the relationship:

$$\Upsilon_c = \frac{\Sigma_c}{E_c} \tag{11}$$

which results in a non-dimensional critical matrix cracking strain of $\hat{\varepsilon}_c = \varepsilon_c / \Upsilon_c = 1.0$, for $\varepsilon_c = \sigma_c/E_m$.

Results were obtained for a representative CVI ceramic matrix plain weave fabric composite with nominal parameters listed in Table 1(a). In the table, the hat (ˆ) notation is used to denote the respective value as non-dimensional consistent with the approach outlined in the previous paragraph. The mesoscopic effective tow elastic properties computed by the hierarchical approach presented in Reference [22] are listed in Table 1(b). The effective inter-tow matrix properties are also listed in the table. Note that a matrix porosity C_{mp} equal to zero is specified in Table 1(a). As a result the effective inter-tow matrix elastic properties are equal to those of the pure matrix material. The unit-cell volume fractions occupied by the mesoscopic phases computed from the matrix layer geometry model surface func-

Table 1. Microstructural, meso-scopic, and unit-cell properties characteristic of a CVI ceramic matrix plain weave fabric composite. The listed properties were obtained using the hierarchical micromechanics model developed in References [22,23].

a) Microstructural Input Parameters

Fiber	Fiber Coating	Matrix	Bundle Coating	Volume Fractions	Geometry
$\hat{E}_f = 0.5$ $\nu_f = 0.2$	$\hat{E}_{fc} = 0.125$ $\nu_{fc} = 0.25$	$\hat{E}_m = 1.0$ $\nu_m = 0.3$	$\hat{E}_{bc} = 0.25$ $\nu_{bc} = 0.25$	$C_f = 0.5$ $C_{fc} = 0.05$ $C_{bm} = 0.1$ $C_{bp} = 0.15$ $C_{bc} = 0.20$ $C_m = 1.0$ $C_{mp} = 0.0$	$\hat{a} = 1.0$ $\hat{b} = 0.1$ $\hat{g} = 0.15$ $\hat{h} = 0.2$ $\hat{l} = 1.0$ $\hat{t} = 0.03$

b) Meso- and Macro-scopic Output

Effective Tow	Effective Matrix	Overall Volume Fractions	Undamaged Unit-Cell
$\hat{E}_{11} = 0.346$ $\hat{E}^{\ell}_{22} = 0.285$ $\hat{G}_{12} = 0.119$ $\hat{G}^{\ell}_{23} = 0.115$ $\nu_{12} = 0.219$ $\nu^{\ell}_{23} = 0.234$	$\hat{E}_{\bar{m}} = 1.0$ $\hat{G}_{\bar{m}} = 0.385$ $\nu_{\bar{m}} = 0.3$	$V_{fill} = 0.272$ $V_{warp} = 0.272$ $V_{matrix} = 0.251$ $V_{void} = 0.204$	$\hat{E}_x = 0.413$ $\hat{E}_y = 0.413$ $\nu_{xy} = 0.261$ $\nu_{yx} = 0.261$ $\hat{G}_{xy} = 0.159$

tions are listed in the third column of Table 1(b). Effective elastic properties of the undamaged unit-cell were computed for the set of mesoscopic properties and geometry using the Rayleigh-Ritz method presented in Reference [19] and are listed in the last column of Table 1(b).

The non-linear response of the matrix material may be characterized through the two parameters ε_s and $\lambda\sigma_c$. Non-linear stress-strain curves for the material system under consideration with different values of the above parameters are presented in Figure 8. In each graph, the unit-cell normalized stress $\hat{\sigma}^\infty$ is plotted against the unit-cell normalized strain $\hat{\varepsilon}^\infty$ for the indicated saturation microcrack density ε_s, and five different magnitudes of the parameter $\lambda\sigma_c$ listed in the lower right corner of the figure. The unit-cell macroscopic response is linear if $\varepsilon_s = 0.0$ or $\lambda\sigma_c = 0.0$, and as such, each graph includes a solid line representing the linear response for the unit-cell with modulus $\hat{E}_x = 0.413$.

For each non-linear curve, a total of 100 strain increments were applied to achieve the final remotely applied unit-cell strain of $\hat{\varepsilon}^\infty = 4.0$. The reported curves were obtained using a 20 × 20 grid of integration stations within each domain element while also using a total of 20 integration stations in the z-direction. Ten series terms were kept in the Rayleigh-Ritz method. Initially the strain was incremented by $\Delta\hat{\varepsilon}^\infty = 0.2$ from zero to reduce unnecessary computation in the linear region without affecting the results. Subsequently, the remaining strain was applied in increments of $\Delta\hat{\varepsilon}^\infty = (4.0 - 0.2)/99$. For every combination of ε_s and $\lambda\sigma_c$, damage initiation occurred at a normalized strain of $\hat{\varepsilon}^\infty = 0.29$ and normalized stress of $\hat{\sigma}^\infty = 0.13$. Damage initiation is a function of the critical matrix microcracking stress σ_c, and the distribution of microstresses prior to the onset of cracking. For these results the stresses are normalized by σ_c, and the same unit-cell microstructure is used in every case. As a result, the initiation is independent of the parameters ε_s and $\lambda\sigma_c$.

If the entire unit-cell value was replaced by fully dense matrix material, the onset of microcracking would occur at a strain of $\hat{\varepsilon}^\infty = \varepsilon^\infty / \varepsilon_c = 1.0$, and stress $\hat{\sigma}^\infty = \sigma^\infty / \sigma_c = 1.0$. The above results indicate that damage initiation occurs in the woven unit-cell at significantly lower remotely applied stress and strain when compared to pure matrix material. This is a direct consequence of the stress concentration near the large scale matrix void, and the non-uniform distribution of unit-cell micro-strain. However, unlike a pure brittle material which may fail catastrophically upon reaching the proportional limit, the matrix cracking in the woven unit-cell is a local event that gives rise to non-catastrophic damage evolution reminiscent of ductility. Hence, although damage initiates at lower strains in the composite material, there is a desirable tendency to resist catastrophic failure beyond the capability of a fully dense brittle matrix counterpart. In this study, a uniaxial strain equal to four times that at which microcracking commences in an otherwise homogeneous tensile specimen comprised of pure matrix material only, is applied to the unit-cell.

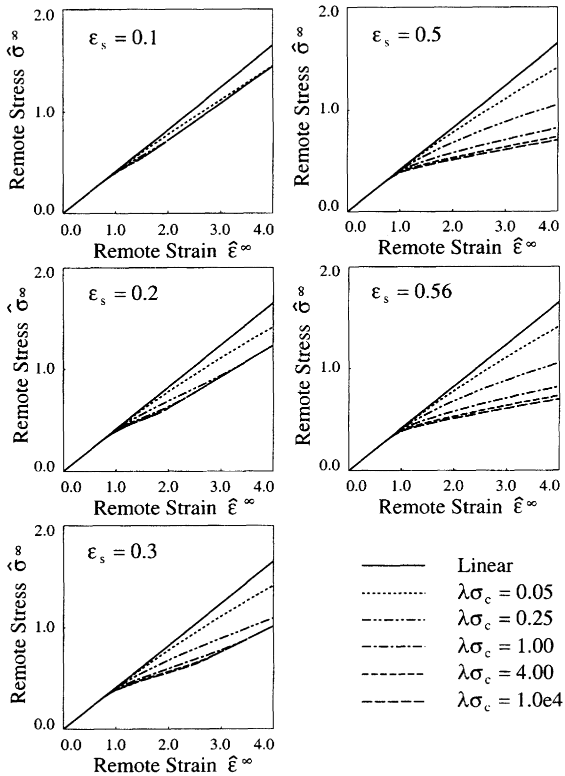

Figure 8. *Simulated non-linear stress-strain curves of the unit-cell with microstructure parameters listed in Table 1 for different values of ε_S and $\lambda\sigma_C$.*

On the Non-Linear Stress-Strain Curves

Some level of non-linear response is apparent in each of the graphs presented in Figure 8. For $\varepsilon_c = 0.1$ there is a brief non-linear response followed by a clear resumption of linearity for all magnitudes of $\lambda\sigma_c$ selected, except peraps the lowest value of $\lambda\sigma_c = 0.05$. The non-linear response for $\varepsilon_s = 0.2$ and 0.3 is expanded, and the resumption of linear response occurs at increased strain. The sequence of linear, non-linear, and again linear response indicates that at these low values of saturation microcrack density, the woven unit-cell matrix material becomes saturated within the range of applied strain. As a result, the local phenomenon is reflected in the macroscopic response. At higher magnitudes of saturation density consisting of $\varepsilon_s = 0.4$ and 0.56, there is no apparent resumption of linearity consistent with the above within the selected range of applied strain. As $\lambda\sigma_c$ becomes large, the stress-strain curve appears to approach a bi-linear form, which is different from the linear resumption previously described.

Aubard et al. [6] presented experimental results for a 2-D SiC/SiC composite with matrix and fiber properties similar to those listed in Table 1(a). The unit-cell geometry is not identified and the system considered does not appear to contain the bundle coating included herein. The total volume percent of matrix (including both inter-tow matrix and bundle matrix) is approximately 40%, and the total volume percent of fiber reinforcements is 40%. Whereas, in the present paper, the total volume percent of matrix and fiber are computed from Table 1(a) as 31% and 27%, respectively. Due to the above differences in microstructure, the system studied herein is significantly more compliant with a normalized elastic modulus $\hat{E}_x = 0.413$ than the composite considered in Reference [6], which has a normalized unit-cell initial modulus of $\hat{E}_x = 0.611$.

Given the differences, and without knowing the details of the unit-cell geometry, it is not possible to do a direct comparison of the results. However, a qualitative comparison of the simulated stress-strain curves with the experimental results presented in Reference [6] can serve to demonstrate the model potential. If the strength of the matrix material coincides with that of Hot Isostatically Pressed (HIP) SiC, we may assume that $\sigma_c = 400$ MPa and $\varepsilon_c = 1.11e - 3$. In the above reference, acoustic emissions were measured during loading and unloading, and matrix cracking was observed to initiate at a normalized stress and strain of approximately $\hat{\sigma}^\infty = 0.2$ and $\hat{\varepsilon}^\infty = 0.3$, respectively. Recall that the corresponding crack initiation stress and strain for the unit-cell considered herein are of $\hat{\sigma}^\infty = 0.13$ and $\hat{\varepsilon}^\infty = 0.29$, respectively. These values are of the same order, and the difference in stress is likely due to the difference in unit-cell stiffness.

In Reference [6], three loading stages were identified by monitoring acoustic emissions. Initially the test coupons underwent linear loading during which there were no acoustic emissions detected, followed by a nonlinear response coinciding with a significant level of acoustic emission counts. As the loading was increased the acoustic emissions stopped at a critical loading and the response was again linear up to ultimate failure. The authors identified the third stage as a "hardening" response dominated by crack opening, and fiber deformation. These three stages are consistent with the linear, nonlinear, and resumed linear response apparent in the curves presented herein. The acoustic emissions ceased at a normalized strain of approximately $\hat{\varepsilon}^\infty = 1.08$, and ultimate failure occurred at a normalized strain of approximately $\hat{\varepsilon}^\infty = 1.8$. Overall, the stress-strain curves presented in Reference [6] appear to be highly consistent with the curves simulated herein (in particular for $\varepsilon_s = 0.3$ and $\lambda\sigma_c = 1.0e4$), differing in scale due to the differences in microstructure. One other difference is in the stage after the saturation stress. The third portion of the curves in Reference [6] do appear to be linear, but are not aligned with a zero stress-strain state. This difference is likely due to other synergistic events such as delamination and frictional fiber pull-out which are not accounted for in this work. A final caveat in comparing the results is that the systems modeled herein are more complex than that studied in Reference [6] and consequently may in all likelihood exhibit more complex load-displacement curves.

Effective Property Degradation

The graphs in Figure 8 contain non-linear stress-strain curves for 25 different combinations of ε_s and $\lambda\sigma_c$. In Figure 9, each of the non-linear stress-strain curves obtained for $\lambda\sigma_c = 1.0e4$, are plotted separately along with the effective elastic properties of the damage unit-cell versus remotely applied strain for five different saturation microcrack density values. The effective properties presented in Figure 9 represent the linear response of the damaged unit-cell at each level of strain. In other words, the reported effective properties represent the slope of the unloading curve as a function of the applied strain and induced damage. The linear in-plane effective properties of the damaged unit-cell were computed in a manner similar to that reported in Reference [20] after the matrix properties were degraded to account for the damage.

As shown in Figure 9, the effective properties of the undamaged unit-cell correspond with the unit-cell elastic properties listed in Table 1(b). Consequently, in each graph at zero normalized strain $\hat{\varepsilon}^{\infty}$, the in-plane Young's moduli $\hat{E}_x$ and $\hat{E}_y$ both equal 0.413, the in-plane Poisson's ratios ν_{xy} and ν_{yx} both equal 0.261, and the in-plane shear modulus $G_{xy} = 0.159$. This set of properties approximately satisfies the relationship $G_{xy} = E_x/[2(\nu_{xy} + 1)]$ indicating that the woven unit-cell is initially bi-directionally isotropic in the plane of the woven composite which applies to all the graphs presented in Figure 9.

As shown in the figure, in all cases presented, the properties remain constant up to the elastic limit, at which point each of the properties appear to decrease. As expected, the degradation of the in-plane effective elastic properties becomes more pronounced with increasing microcrack saturation level ε_s. At low ε_s, which reflects the material's ability to microcrack at only relatively low levels, the degraded properties at high levels of applied strain are predicted to be moderately smaller (about 5–10%) than the properties of the virgin unmicrocracked matrix phase. Also at low ε_s values, and although these results were obtained for a system loaded in tension along its x-axis, an equal reduction in both E_x and E_y is predicted. On the other hand, the results obtained for higher saturation densities suggest that, during loading, the evolution of microcrack damage in the uniaxial loading case under consideration degrades the effective modulus in the direction of loading at higher rates when compared to its orthogonal counterpart. A wide range of simulation reported elsewhere [34] suggests that this effect is predicted to be stronger at higher ε_s values and it is most pronounced for $\lambda\sigma_c = 1.0e4$ and $\varepsilon_s = 0.56$ reported in Figure 9.

While damage induced orthotropies should indeed be expected in such highly

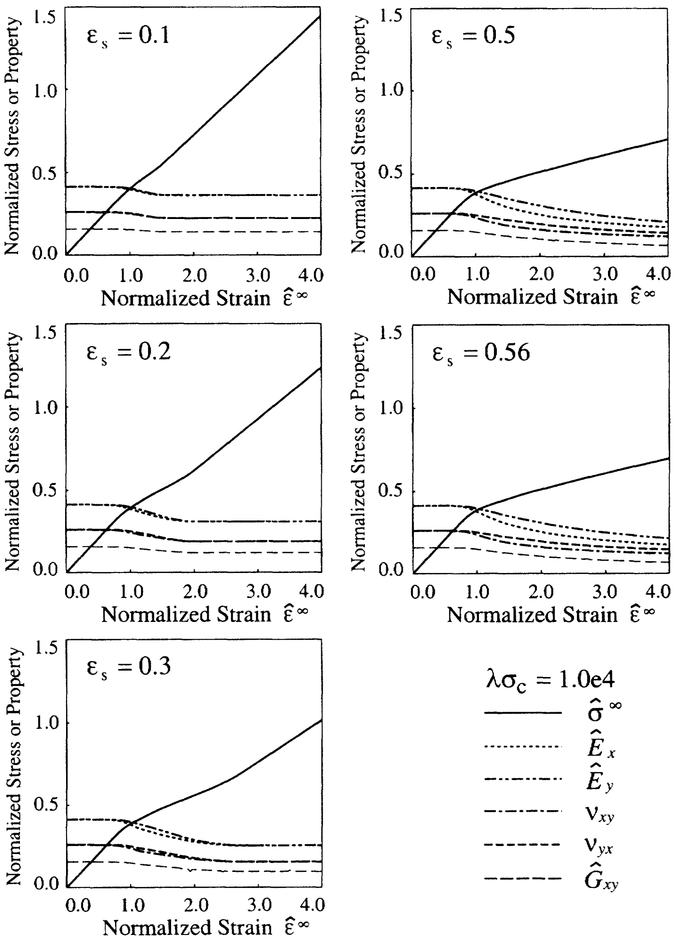

Figure 9. *Non-linear response and effective properties of the damaged unit-cell versus remote strain for $\lambda\sigma_c$ = 1.0 e4.*

complex systems, the isotropic matrix microcracking model employed herein does not appear to be capable of fully capturing such effects. In the extreme case for example, wherein the applied loads are sufficiently high to cause the matrix phase to fully microcrack to its saturation level, the isotropic matrix microcracking model used in this study would predict equal degradation of the effective elastic properties in the x and y direction although the loading is only applied in the x direction. Such a prediction is clearly counter-intuitive and may also be of theoretical interest only. Thus, while the model appears to capture some of the damage induced orthotropies prior to damage saturation during uniaxial loading, the convergence of the effective moduli curves with further load increases should be viewed critically as reflective of the model's limitation. Other limitations of the microcracking model such as its limited effectiveness to account for microcrack proximity and crack closure effects especially at higher microcrack densities, i.e., $\varepsilon > 0.4$ should also be noted as needed for the appropriate use of the reported results.

Damage Zones

In order to better understand the progression of damage in the woven unit-cell, a 20-node 3-D brick finite element mesh was used for the sole purpose of displaying fringes of the matrix microcrack density ε. Within each layer, at a given state of remotely applied strain, the damage values stored at the $8 \times M \times N \times n_z$ Gaussian integration stations were used to degrade the matrix properties uniformly through the thickness of each layer. The Kuhn and Charalambides semi-analytical method was used to compute the elastic microstrain field of the damaged unit-cell. The resulting finite series solution was used to compute the local strains at each node in the finite element mesh. This distribution of strain, which varies through the depth, was used to recompute the local damage at each node. The above procedure was used to compute unit-cell fringes at four points along the stress-strain curve for $\varepsilon_s = 0.5$ and $\lambda\sigma_c = 4.0$ shown in Figure 10. The resulting fringes are presented in Figures 11–12.

The above sequence of microcrack density fringes offers insight into the progression of damage in the unit-cell matrix material. Figure 11 corresponds with point a in Figure 10, which falls after damage initiation but before the characteristic "knee" in the stress-strain curve. At this point the inter-tow matrix material has sustained appreciable damage, and damage has also initiated in the matrix material of both the warp and fill tows. Recall that this point is well below the proportional limit of pure matrix material, but does not result in catastrophic failure because the damage under consideration is a local event occurring in only the matrix phase of an otherwise undamaged woven unit-cell.

In Figure 12, which corresponds with point b in Figure 10, the inter-tow matrix material has a distinct band of highly damaged material. Even though the damage

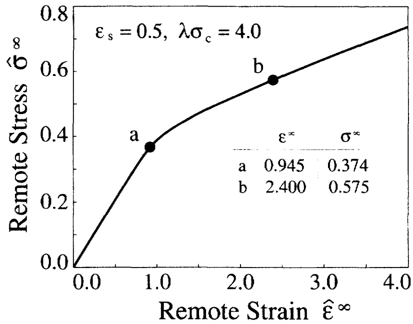

Figure 10. *Non-linear stress-strain curves* ε_s *= 0.5 and* $\lambda\sigma_c$ *= 4.0.*

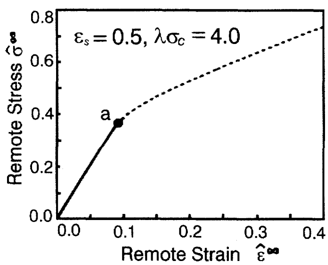

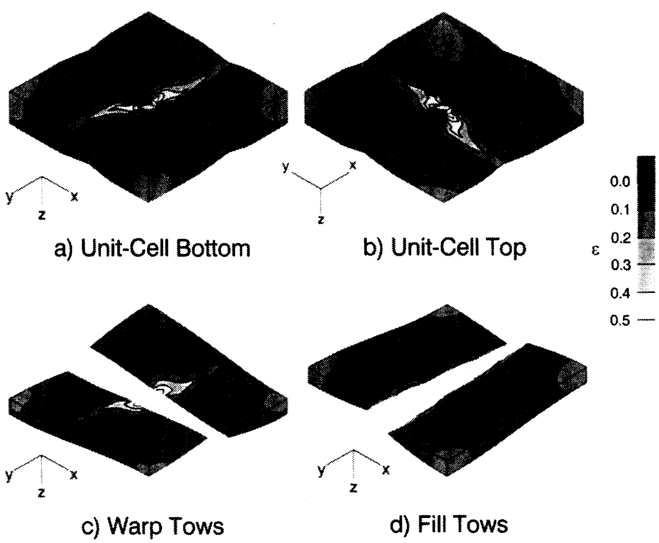

Figure 11. *Fringes of the microcrack density* ε*, after damage initiation, corresponding to load point* a.

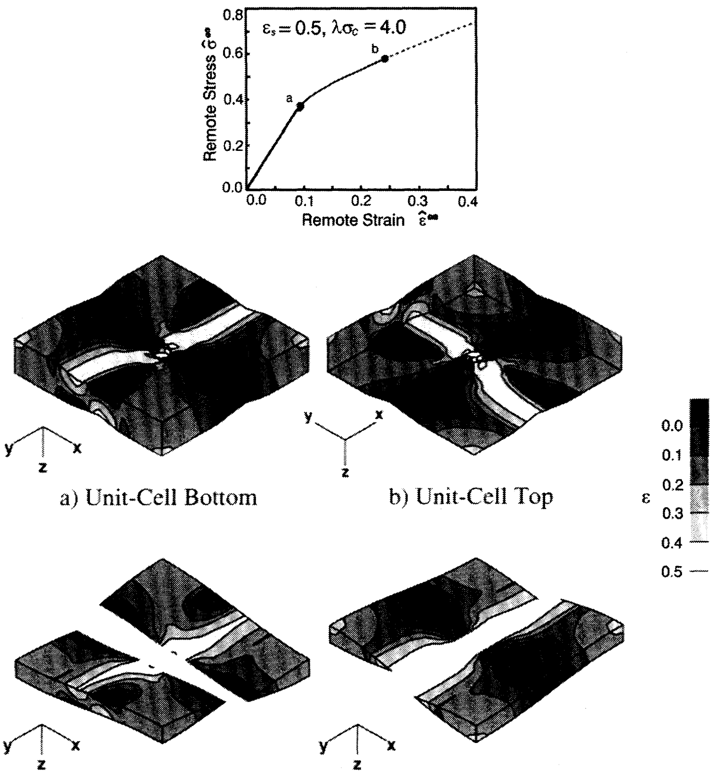

Figure 12. *Fringes of the microcrack density* ε, *associated with loading point* b.

is saturated only near the hole, the matrix material sustains significantly reduced load. As a result, most of the load is transferred through the fiber reinforcements and the warp tows. This essentially simulates the evolution of a matrix crack in the fill tows bridged by the tow fiber reinforcements.

Kuo and Chou [15] studied the effects of transverse bundle cracking and Inghels and Lamon [2] employed the Aveston and Kelly [33] theory to model the normal bundle matrix cracking perpendicular to the fiber direction. The former represents the primary mode of failure in the fill tows, and the latter coincides with the primary mode of failure in the warp tows under unidirectional loading in the warp direction. In all cases it appears that failure initiates in the inter-tow matrix and damage progresses into the tows. It is not clear from the literature which type of bundle matrix cracking is dominating or occurs first. The simulations presented herein show that during uniaxial loading, normal bundle matrix cracking is slightly more prevalent than the transverse bundle cracking. However, the order and extent appears to be highly dependent on the microstructure. In particular, increased bundle porosity results in greater dissimilarity between the longitudinal and transverse moduli of the tows. This results in greater micro-beading and stress concentrations at the corners of the unit-cell, which may enhance transverse bundle matrix cracking. Conversely, lower bundle porosity could also result in less damage at the unit-cell corners, causing the normal bundle matrix cracking of the warp tows to prevail. In this work, the volumetric effect of the micro-porosity on the effective properties of the fiber bundles was indeed taken into account, but the micro-stress concentrations due to the micro-porosity was not accounted for. In order to account for such micro-stress concentrations due to micro-porosity, and also account for other potentially concurrent micro-failures, the present level of analysis will need to be further refined and expanded. While such complementary modeling efforts are currently under way, the findings of this study, despite its many limitations, may also assist in the development of a better understanding of the mechanical response of CMC woven composites whose behavior is rather complex and difficult to characterize.

CONCLUSIONS

Woven brittle matrix composites are unique because the intertwined bundles of fibers help to arrest crack growth in the matrix material. While unidirectional composites rely mostly on frictional fiber pull-out, woven composites exhibit substantial controlled load matrix cracking. Because the matrix material contribtes significantly to the stiffness of the woven composite, the non-linearities may be dominated by mechanisms associated with failure of the brittle matrix material.

This work represents a first step attempt to simulate, through a continuum microcracking model, the anisotropic non-linear response of brittle matrix woven composites. An iterative approach based on hierarchical micromechanics and relatively accurate linear microstrain estimates was used to model the non-linear response under uniaxial tension. Numerical simulations were completed for a representative brittle matrix woven composite with highly complex microstructure including a discrete large scale macroscopic void in the inter-tow matrix phase. The damage parameters ε_s and $\lambda\sigma_c$ were varied and for each set of values the non-linear uniaxial stress-strain curve was traced. For each case the effective linear elastic unit-cell properties were computed for the damaged unit-cell at each state of strain. The results revealed an orthotropic unit-cell response in the non-linear region. The distribution of damage at four points along a single stress-strain curve was also investigated. The presence of damage accumulation reminiscent of mode I matrix cracking in the warp tows, transverse matrix cracking in the fill tows, and dispersed microcracking in the matrix phase between tows was observed. The results were qualitatively compared with results for a similar but less complex system presented by Aubard et al. [6]. The trends and overall behavior compare favorably.

The isotropic microcracking model employed herein is associated with several limitations. This includes its reduced sensitivity in assessing directional property degradation during loading and its limited capacity to account for microcrack proximity effects at microcrack densities higher than 0.4. The simplicity of the model, however, and its surprising predictive capabilities that encompass a wide range of non-linear stress-strain responses and damage evolution may render this model rather useful in predicting the non-linear response of woven CMC composites with complex microstructures.

ACKNOWLEDGMENTS

Support for this work was provided by the National Science Foundation, Grant No. CMS94-96209. Useful discussions with Professors Frank Zok and Rajendra Bordia are gratefully acknowledged.

REFERENCES

1. E. Inghels and J. Lamon. "An Approach to the Mechanical Behaviour of SiC/SiC Ceramic Matrix Composites: Part 1—Experimental Results." *J. Mater. Sci.,* 26:5403–5410, 1991.
2. E. Inghels, and J. Lamon. "An Approach to the Mechanical Behaviour of SiC/SiC Ceramic Matrix Composites: Part 2—Theoretical Approach." *J. Mater. Sci.,* 26:5411–5419, 1991.
3. Z. G. Wang, C. Laird, Z. Hashin, B. W. Rosen, and C.-F. Yen. "Mechanical Behaviour of a Cross-Weave Ceramic Matrix Composite: Part I, Tensile and Compressive Loading." *J. Mater. Sci.,* 26:4751–4758, 1991.
4. J. Lamon, N. Lissart, C. Rechiniac, D. H. Roach, and J. M. Jouin. "MIcromechanical and Statistical Approach to the Behavior of CMC's." *Ceram. Engr. Sci. Proc.,* 14:1115–1124, 1993.
5. W. S. Steffier. "The Orthotropic Mechanical Behavior of Nicalon Fiber-Reinforced SiC-Matrix Composites." *Ceram. Engr. Sci. Proc.,* 14(9–10):1045–1057, 1993.
6. X. Aubard, J. Lamon, and O. Allix. "Model of the Nonlinear Mechanical Behavior of 2D SiC-SiC Chemical Vapor Infiltration Composites." *J. Amer. Ceram. Soc.,* 77(8):2118–2126, 1994.
7. J. P. Singh, S. Singh, and R. A. Lowden. "Effect of Fiber Coating on Mechanical Properties of Nicalon Fibers and Nicalon-Fiber/SiC Matrix Composites." *Ceram. Engr. Sci. Proc.,* 15(4):456–464, 1994.
8. X. Aubard. "Modelling of the Mechanical Behaviour of a 2-D SiC-SiC Composite at a Meso-Scale." *Composites Sci. & Tech.,* 54:371–378, 1995.
9. R. K. Bordia, D. H. Roach, S. M. Salamone, and M. Headinger. "Tensile Properties and Crack Growth Resistance of Ceramic Matrix Composites." Submitted to *J. Amer. Ceram. Soc.*
10. J. C. McNulty and F. W. Zok. "Notch Sensitivity of SiC/SiC at Ambient and Elevated Temperatures." April, 1996. Presented at *The American Ceramic Society 1996 Annual Meeting & Exposition,* Indianapolis, Ind.
11. S. V. Nair and Y.-L. Wang. "Failure Behavior of a 2-D Woven SiC Fiber/SiC Matrix Composite at Ambient and Elevated Temperatures." *Ceram. Engr. Sci. Proc.,* 13(7–8):433–441, 1992.
12. R. K. Bordia, D. H. Roach, and S. M. Salamone. "Crack Growth Resistance of CVI Processed Ceramic Matric Composites." *Proceedings of ICCM,* 1995.
13. T. E. Steyer and F. W. Zok. "Stress Rupture of an SiC/SiC Composite." April 1996. Presented at The *American Ceramic Society 1996 Annual Meeting & Expositions,* Indianapolis, Ind.

14. W.-S. Kuo and T.-W. Chou. "Modeling of Nonlinear Constitutive Relations of Woven Ceramic Composites." *Ceram. Engr. Sci. Proc.*, 12(7–8):1556–1573, 1991.
15. W.-S. Kuo and T.-W. Chou. "Elastic Response and Effect of Transverse Cracking in Woven Fabric Brittle Matrix Composites." *J. Amer. Ceram. Soc.*, 78(3):783–792, 1995.
16. D. M. Blackketter, D. E. Walrath, and A. C. Hansen. "Modeling Damage in a Plain Weave Fabric-Reinforced Composite Material." *J. Composite Tech. & Res.*, 15(2):136–142, 1993.
17. A Dasgupta and S. M. Bhandarkar. "Effective Thermomechanical Behavior of Plain-Weave Fabric-Reinforced Composites Using Homogenization Theory." *J. Engr. Mater. & Tech.*, 116:99–105, January 1994.
18. K. Woo and J. D. Whitcomb. "Three-Dimensional Failure Analysis of Plain Weave Textile Composites Using a Global/Local Finite Element Method." *J. Composite Mater.*, 30(9):984–1003, 1996.
19. J. L. Kuhn, S. I. Haan, and P. G. Charalambides. "A Semi-Analytical Method for the Calculation of the Elastic Micro-Fields in Plain Weave Fabric Composites Subjected to In-Plane Loading." *J. Composite Mater.*, 33(3)221–266, 1999.
20. S. I. Haan, J. L. Kuhn, and P. G. Charalambides. "Elastic Response of Plain Weave Ceramic Matrix Composites Under Remote In-Plane Loading." *J. Amer. Ceram. Soc..*, January, 1999, in revision.
21. J. L. Kuhn and P. G. Charalambides. "On the Accuracy of Approximate Elastic Microfields in Plain Weave Fabric Composites Under In-Plane Loading." Submitted to *J. Composite Mater.* November, 1997, in revision.
22. J. L. Kuhn and P. G. Charalambides. "Elastic Response of Porous Matrix Plain Weave Fabric Composites: Part I—Modeling." *J. Composite Mater.*, 32(16):1426–1471, 1998.
23. J. L. Kuhn and P. G. Charalambides. "Elastic Response of Porous Matric Plain Weave Fabric Composites: Part II—Results." *J. Composite Mater.*, 32(16)1472–1507, 1998.
24. J. L Kuhn and P. G. Charalambides. "Modeling of Plain Weave Fabric Composite Geometry." *J. Composite Mater.*, 33(3)188–220, 1999.
25. S. I. Haan, J. L. Kuhn, and P. G. Charalambides. "Elastic Micro-Fields and Effective Properties of Polymer Matrix Plain Weave Fabric Composites." In progress.
26. P. G. Charalambides and R. M. McMeeking. "Finite Element Method Simulation of Crack Propagation in a Brittle Microcracking Solid." *Mech,. of Mater.*, 6:71–87, 1987.
27. P. G. Charalambdies and R. M. McMeeking. "Near-Tip Mechanics of Stress-Induced Microcracking in Brittle Materials." *J. Amer. Ceram. Soc.*, 71(6):465–472, 1988.
28. B. Budiansky and R. J. O'Connell. "Elastic Moduli of a Cracked Solid." *I. J. Sol. & Struc.*, 12:81–97, 1976.
29. Y. Fu and A. G. Evans. "Some Effect of Microcracks on the Mechanical Properties of Brittle Solids—I. Stress, Strain Relations." *Acta Metall.*, 33(8):1515–1523, 1985.
30. Z. Hashin. "Analysis of Composite Materials—A Survey." *J. Appl. Mech.*, 50:481–505, September 1983.
31. J. L. Bassani. "Linear Densification and Microcracking in Sintering Compacts." In *Mech. of Mater.*, vol. 12, pp. 119–130. Elsevier Science Publishers B.V., 1991.
32. D. B. Marshall, B. N. Cox, and A. G. Evans. "The Mechanics of Matrix Cracking in Brittle-Matrix Fiber Composites." *Acta Metall.*, 33(11):2013–2021, 1985.
33. J. Aveston and A. Kelly. "Theory of Multiple Fracture of Fibrous Composites." *J. Mater. Sci.*, 8:352–362, 1973.
34. J. L. Kuhn. "Mechanical Behavior of Woven Ceramic Matric Composites." Ph.D. Thesis, Department of Mechanical Engineering, The University of Maryland Baltimore County, Baltimore, MD 21250. January 1998.